Biosystems Engineering (2007) **96** (2), 231–237
doi:10.1016/j.biosystemseng.2006.10.018
PH—Postharvest Technology

Stem-end/Calyx Identification on Apples using Contour Analysis in Multispectral Images

J. Xing[1,2]; P. Jancsók[2]; J. De Baerdemaeker[2]

[1]Department of Bioresource Engineering, McGill University Macdonald Campus, 21,111 Lakeshore Road, Ste-Anne-de-Bellevue, Que., Canada H9X 3V9
[2]Division of Mechatronics, Biostatistics and Sensors, Department of Biosystems, Catholic University of Leuven, Kasteelpark Arenberg 30, B-3001 Leuven, Belgium; e-mail of corresponding author: juan.xing@gmail.com

(Received 8 October 2005; accepted in revised form 27 October 2006; published online 9 January 2007)

As a part of a project concerned with detecting bruises on 'Golden Delicious' and 'Jonagold' apples, a hyperspectral imaging system was used for separating stem-end/calyx regions from true bruises. Based on principal component analysis (PCA) of the hyperspectral images, multiple effective wavebands were selected. Afterwards, PCA and image-processing techniques were applied to the multispectral images. The stem-end/calyx regions were identified and distinguished from the cheek surfaces by analysing the contour features of the first principal component score images. None of the sound tissue was misclassified as a stem-end or calyx region for both cultivars apples. In the investigated samples, all of the stem-end/calyx presented in the images were correctly recognised for the 'Golden Delicious' apples and 98·33% for 'Jonagold' apples. Less than 3% of bruises were misclassified as stem-end/calyx regions for both cultivars apples.

1. Introduction

Appearance is an important quality index of apples to consumers (Röhr *et al.*, 2005). It is important to separate the damaged fruits from the sound ones. This not only increases the marketability but also enhances or maintains the shelf life of the products. For example, the presence of mechanical damage accelerates spoilage of harvested products. Effective removal of damaged products may maintain the quality of the entire lot until it reaches the consumers. Machine vision systems have received much attention for sorting apples into different categories according to size and colour; however, they still have some limitations in surface defect detection (Lu, 2003; Leemans & Destain, 2004). In the images, normally, the defective surface has a lower reflection than healthy tissue on the uniform colour apple such as 'Golden Delicious'. Since the stem-end or calyx regions also have less reflection compared to the cheek surfaces, they might be misrecognised as defects as a consequence. The situation is more complicated in 'Jonagold' apples, on which the blushed healthy tissue could have even lower reflection than the bruises on the green cheeks. The natural colour variation makes the sorting more difficult.

Therefore, the identification of the stem-end/calyx from the true defects became a part of our project concerning bruise detection on apples. Bennedsen and Peterson (2005) configured a machine vision system to detect the surface defects on apples. In their system the first step was to determine the orientation of the apples. The image of apple would be processed only when the stem-end-calyx axis is perpendicular to the imaging camera. With respect to the detection of the stems on fruits, Wolfe and Sandler (1985) developed an algorithm based on syntactic analysis of angle patterns in the stem. However, this method would be inefficient if the stem does not appear as a protrusion in the images. Ying *et al.* (2003) proposed an algorithm to detect the stem and shape of pears. The stem was also assumed as a protrusion of the sphere fruits. These efforts were made mainly for detecting the length of stems instead of the confusion between stem-end regions and defects. In order to separate the stem-end and calyx regions from the true defects on apple, Yang (1993) established a structured lighting arrangement. Through the analysis

of the laser line pattern it is possible to determine whether the suspected region is a true defect. Wen and Tao (2000) distinguished the true defects from the stem-end/calyx of fruit by using dual-camera (near infrared and mid-infrared) images. The bruised area and stem-end/calyx have different responses to the cameras, so that the stem-end/calyx is able to be distinguished from the surface defects by simple comparison of two images. Cheng *et al.* (2003) used the same arrangement for on-line stem-end/calyx recognition. They pointed out that the inspection accuracy might be affected by the temperature distribution on the surface of the test samples. In Leemans *et al.* (2002), the calyx and stem-end, which appeared on an image as defects, were detected using a correlation pattern recognition technique. Prior to using this technique, a library had to be created. Kavdir and Guyer (2004) used texture features of apple images to distinguish the difference between the defective and good apples. Confusion between the stem-end/calyx was considered. Good results were obtained for some varieties of apples.

Recently, hyperspectral imaging system has been developed for the food quality and safety control (Kim *et al.*, 2001; Chao *et al.*, 2002; Park *et al.*, 2002; Ma & Tao, 2005). The inspection speed is one main constraints for applying it in an on-line system. Therefore, in most of the cases, multispectral imaging is preferred where only a limited number of wavebands are inspected. Most of the research on apples focuses on detecting the surface contamination on cheeks (Lu, 2003; Mehl *et al.*, 2004; Xing *et al.*, 2005). Using a hyperspectral imaging system, many more images at different wavebands can be recorded than with the conventional camera; also because of the possibility of combining chemometrics with image-processing techniques, it has the potential to identify the stem-end/calyx regions from the cheek surfaces of apples by analyzing hyperspectral or multispectral images.

Therefore, the objectives of this research are:

(a) to construct a hyperspectral imaging system, and subsequently build a multispectral imaging system and
(b) to develop an algorithm to identify the stem-end/calyx and distinguish it from the cheek surfaces, whether damaged or intact.

2. Materials and methods

2.1. *Sample preparation*

In this study, 94 'Golden Delicious' and 187 'Jonagold' apples were purchased from a local supermarket. In the laboratory, they were separated into non-bruised and bruised group by thorough visual inspection. Most of the existing bruises could be found on the cheeks and showed the typical browning symptoms. For research purposes, more bruises were induced by a pendulum on the cheeks along the equator as well as on the surfaces around calyx or stem-end regions. The impact energy used to bruise the apples was about 0·15 J. The images were taken 1 day after bruising. The apples used for stem-end/calyx imaging were picked up randomly from the apples under investigation (52 from 'Golden Delicious' apples and 60 from 'Jonagold' apples).

2.2. *Hyperspectral imaging system*

The developed hyperspectral imaging system [*Fig. 1(a)*] is composed of four sections: a sample transportation plate, two 150 W halogen lamps, an ImSpec V10 spectrograph (spectral Imaging Ltd., Oulu, Finland) coupled with a standard C-mount zoom lens (Cosmicar H6Z810), and a Hitachi KP-F120 monochrome camera. The wavelength region the system can sense is between 400 and 1000 nm.The camera and spectrograph were used to scan the apples line-by-line as the transportation plate moved the apples through the field of view of the optical system (as illustrated in [*Fig. 1(b)*]). A hyperspectral image can be recorded for each scan. The resolution of the image acquisition system was 800 by 1040 pixels by 10 bits (800 in the spatial and 1040 in the spectral directions), which corresponds to a spatial resolution of 0·15 mm and a spectral resolution of 0·7 nm. The step size of the precise linear motion table was set as 0·5 mm. After finishing scanning for an entire fruit, a data cube can be obtained.

For the hyperspectral imaging system, the wavelength calibration equation used is

$$\lambda_p = 0{\cdot}6306p + 340{\cdot}55 \tag{1}$$

where p is the pixel position in the image and λ_p is the wavelength in nm corresponding to the pixel position p of the image.

Reflectance R is calibrated using equation

$$R = \frac{I_{im} - I_{dark}}{I_{ref} - I_{dark}} \tag{2}$$

where: I_{im} is the intensity of an image; I_{ref} is the intensity of the standard 99% reference (Spectralon, Labsphere Inc.); and I_{dark} is the intensity of the dark image, which was measured by closing the chamber, turning off all light sources and covering the lens with a black cap.

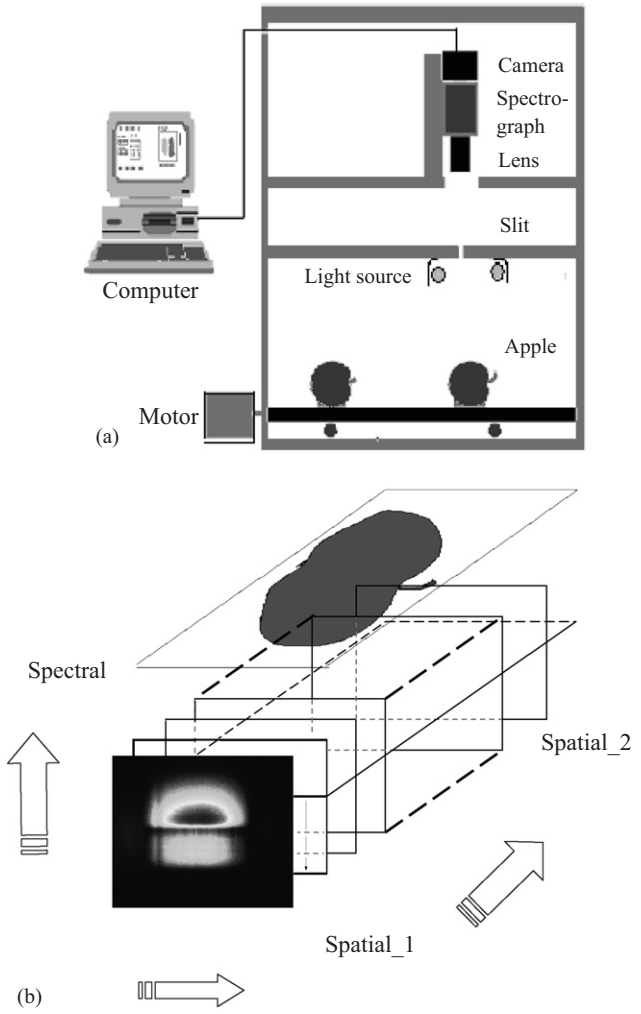

Fig. 1. Schematic of hyper-spectral imaging system (a) and its working principle (b)

2.3. *Data processing and analysis*

The image capture program was written in Labview v7.1 (National Instrument Corporation, Austin, USA) while the processing program was developed in Matlab v6.5 (The MathWorks Inc., Natick, USA).

In the first step, to reduce the noise and amount of data for calculation, the spatial-spectral data from each scan were decreased to 160 by 104 by averaging the neighbouring pixels.

In a hyperspectral image, each pixel on apple surface corresponds to a reflectance spectrum in the range of 400–1000 nm. To avoid low signal to noise ratio, only wavelength range from 500 to 900 nm was used in this investigation. In order to summarise the information contained in the spectra, principal component analysis (PCA) was used. The purpose of this technique is to obtain an overview of all the information in the data set. It summarises data by forming new variables, which are uncorrelated and linear combinations of the original variables. A few of these new variables (principal components) represent the larger part of the common variations to all the data. By only considering several principal components, the high-dimensional spectral data can be reduced to a lower dimensionality with a minimal loss of information. A score is the estimated value for a principal component (PC). Each spectrum has a score along each PC. In this study, PCA image scores were not only used to aid in visualising the hyperspectral data, but also to select optimal wavebands for multispectral imaging. Principal component analysis was performed on the dataset after reflectance calibration. Only the spectra corresponding to the pixels on an apple were investigated.

3. Results and discussion

3.1. *Principal component analysis on the full wavelength region*

Principal component scores images were constructed by replacing the intensity or reflectance value of the pixels in images with the score value of each principal component (Xing *et al.*, 2005). As it is well known, the first PC gives the grey-level information of the sample. Due to the construction of the light source used in this arrangement, it seems that the first principal component (PC1) scores image also demonstrates the uneven illumination conditions (shown in the second row of *Fig. 2*). It may be caused by the different distances from the apple surface to the light source. There are no significant characteristics related to the presence/absence of bruises on the apple, nor to the skin colour information. This can be clearly seen from the example of 'Jonagold' apple. The images in the first row of *Fig. 2* are the pseudocolour images of the example 'Golden Delicious' and 'Jonagold' apple. Apparently, there are two skin colours on the 'Jonagold' apple. However, the effect of skin colour on the PC1 scores image is not observable. The second principal component (PC2) may display more information related to the skin colour.

For the 'Golden Delicious' apples, PC2 or PC3 (the third principal component) scores images are more related to the presence or absence of bruises on apple. Since PC2 may represent the information associated with skin colour, it is assumed that the PC2 scores image displays the browning symptom of the bruised tissue. The PC3 scores image might account for the other features of bruised tissue on 'Golden Delicious' apples. For example, when the tissue was severely damaged, the

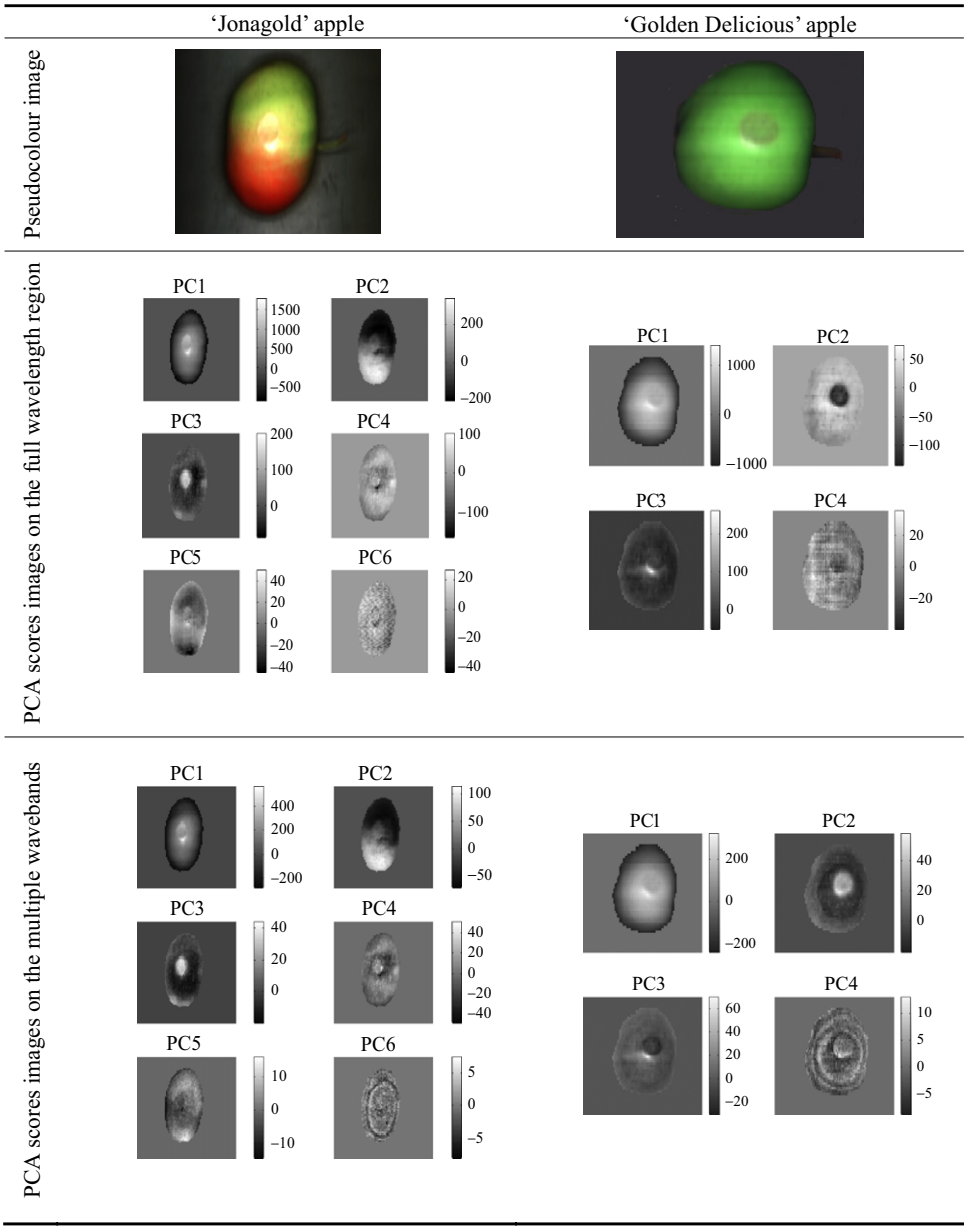

Fig. 2. Principal component analysis (PCA) scores images for the full wavelength range and selected wavebands; PC1,PC2, PC3 and PC4 is the 1st, 2nd, 3rd and 4th principal component, respectively

bruised area would be very likely detectable in the PC2 scores image because of the significant discoloration; otherwise, it might be evident in the PC3 scores images. For the 'Jonagold' apple, more principal components are necessary for determining the presence/absence of bruises due to the natural skin colour variations. Normally, the bruises can be indicated in one of the first six PC scores images. However, it is difficult to find interpretations for the third–sixth principal components.

3.2. *Principal components analysis on the multiple wavebands*

Since the main aim of the research is bruise detection, the effective wavebands were chosen according to the analysis of the images for bruised apples. According to the loading plots, four wavebands for 'Golden Delicious' apples were identified. They are centred at 558, 678, 728 and 892 nm, respectively (Xing *et al.*, 2005). Similarly, six wavebands for 'Jonagold' apples were

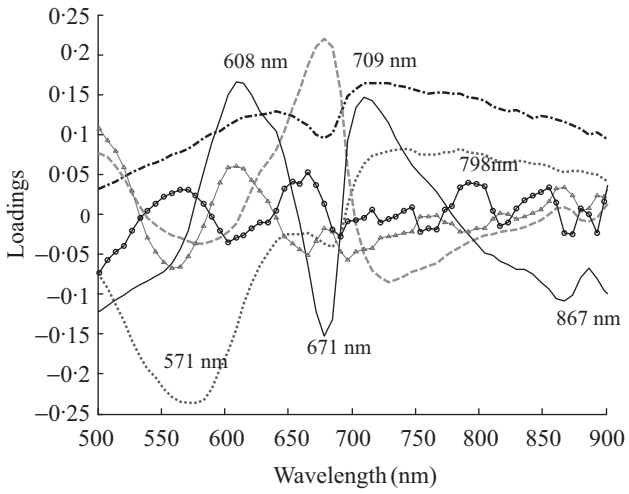

Fig. 3. Loading plots of 'Jonagold' apples; ----, the first principal component; ·····, the second principal component; – – –, the third principal component; ——, the fourth principal component; ——△——, the fifth principal component; ——○——, the sixth principal component

selected: 571, 608, 671, 709 798 and 867 nm (shown in *Fig. 3*).

Principal component analysis procedure was then repeated on the selected multiple optimal wavebands instead of the full wavelength range. As can be seen in the third row of *Fig. 2*, the PCA images obtained from the multiple wavebands give very similar results as from the full wavelength region. Therefore, the later image processing was for the PCA image scores obtained from the selected wavebands.

3.3. *Stem-end/calyx regions identification*

As noticed, the PC1 scores image reveals the distance of sample surface to the light source, which means it might be good for studying the geometric information of sample surfaces. It is an obvious advantage for recognising the stem-end/calyx regions since they introduce concavities in the overall convex shape of apples. Moreover, the PC1 scores images are independent of

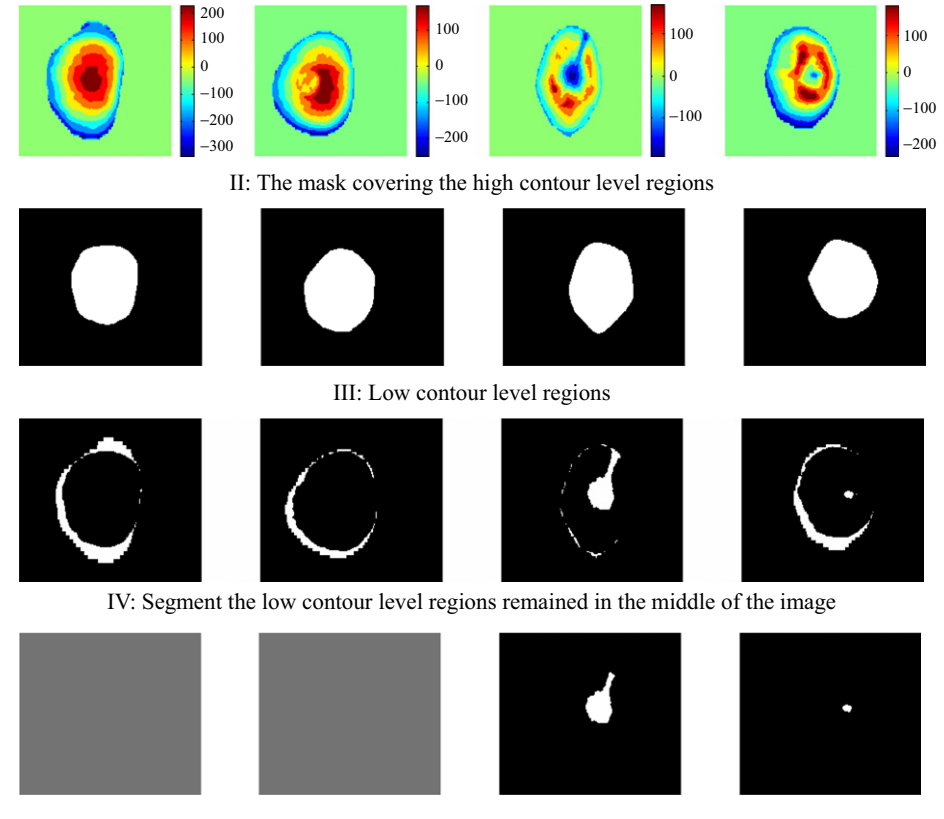

Fig. 4. Flow chart showing the procedures used to identify stem-end/calyx on apples

skin colour of an apple. It implies that it is not necessary to take the skin colour into account while developing a classification algorithm. The skin colour variation is a typical problem for working with bicoloured apples such as 'Jonagold' using machine vision.

Since the apple has a nearly spherical surface, on the smooth intact cheeks, the contour lines should be approximately in parallel. The presence of bruises or stem-end/calyx may make the shapes of contour lines irregular. This is one of the hypotheses for developing the classification algorithm. The first row of *Fig. 4* shows the filled contour images of four apples: healthy, bruises on cheek, stem-end, and calyx with a bruise nearby. The filled contour images were created by using 'contourfill' command in MatLab. The colour in the image indicates the intensity value not the colour of the skin. The region of each contour level has a nearly regular and circular shape on the cheek of healthy apple, but this does not hold true for the images with bruise or stem-end/calyx. For the images with a calyx or stem-end region, the lowest contour regions can be observed in the middle area of the image. Moreover, in most of the situations, the stem-end or calyx region is surrounded by regions with higher intensities, which was hardly observed in the images of bruises or healthy cheeks. This is the second hypothesis for developing the identification algorithm.

Figure 4 shows photographically the procedures to identify stem-end/calyx regions. In the first step the filled contour images were prepared for later processing. The number of the contour levels was defined as 8. In step 2, mask images were created. The masks were formed by using morphological methods to the regions, which cover the first four highest contour levels of each apple (second row of *Fig. 4*). In step 3, the regions, which cover the two lowest contour levels of each apple, were identified (shown in the third row of *Fig. 4*). Finally, an *'and'* operation was applied to the pictures obtained in steps 2 and 3 (shown in the bottom row of *Fig. 4*). A 'clean' morphological operation was carried out to remove small areas, which may be the noise from the optics, or from the pigments on the apple surface. If there is a big area retained in the resulting image, it, most probably, is an image with a calyx or stem-end region. Otherwise, it is an image of apple cheek, whether bruised or not.

The total recognition rates for stem-end and calyxes are shown in Table 1. For 'Golden Delicious' apples, all of the stem-end/calyx regions were correctly identified. A 100% of classification accuracy was achieved for the calyxes of 'Jonagold' apples too. Only one image with presence of stem-end region was misclassified for 'Jonagold' apple. In the error case, the stem-end region was at the edge of the image and the mask cut off part of the surrounding areas. Less than 3% bruised cheeks from both cultivars apples were misclassified as calyx or stem-end regions. No error was observed between the healthy cheeks and stem-end/calyx regions. Concerning the separation between the sound and bruised tissue on apple cheeks, please refer to Xing *et al.* (2005).

Table 1
Classification results

Feature	*Class*	
	Stem-end/calyx	*Not stem-end/calyx*
'Golden Delicious' apples:		
Healthy ($n = 48$)	0	48 (100%)
Bruises ($n = 46$)	1	45(97·83%)
Calyx ($n = 28$)	28 (100%)	0
Stem-end ($n = 24$)	24 (100%)	0
'Jonagold' apples		
Healthy ($n = 65$)	0	65 (100%)
Bruises ($n = 122$)	3	119(97·54%)
Calyx ($n = 30$)	30 (100%)	0
Stem-end ($n = 30$)	29 (96·67%)	1

n, number of samples.

4. Conclusions

A hyperspectral imaging system has been built for studying the surface quality of apples. The main goal of the project is to efficiently detect bruises on apples. Based on the analysis of the hyperspectral images in the full wavelength region (500–900 nm), four and six effective wavebands were chosen for detecting bruises on 'Golden Delicious' and 'Jonagold' apples, respectively. After that, these selected wavebands were also expected to be useful for recognising the stem-end/calyx from the cheek surface. Principal component analysis (PCA) was considered to summarise the multispectral information. The algorithm to identify the stem-end/ calyx on apples was developed on the basis of the contour features in the PCA image scores. Test results show that the system can effectively identify stem-end/calyx regions and distinguish them from bruised regions on 'Jonagold' and 'Golden Delicious' apples. Further enhancement of classification results and robustness can be achieved by improving the mask formation and using a more sophisticated strategy for discrimination. Future work also includes integration the algorithm of detecting bruises on apple cheeks with the identification of the stem-end/calyx.

Acknowledgements

The authors gratefully acknowledge the financial support of the Catholic University of Leuven.

References

Bennedsen B S; Peterson D L (2005). Performance of a system for apple surface defect identification in near-infrared images. Biosystems Engineering, **90**(4), 419–431

Chao K; Mehl P M; Chen Y R (2002). Use of hyper-and multi-spectral imaging for detection of chicken skin tumors. Transactions of the ASAE, **18**(1), 113–119

Cheng X; Tao Y; Chen Y R; Luo Y (2003). NIR/MIR dual sensor machine vision system for online apple stem-end/calyx recognition. Transactions of the ASAE, **46**(2), 551–558

Kavdir I; Guyer D E (2004). Comparison of artificial neural networks and statistical classifiers in apple sorting using textural features. Biosystems Engineering, **89**(3), 331–344

Kim M S; Chen Y R; Mehl P M (2001). Hyperspectral reflectance and fluorescence imaging system for food quality and safety. Transactions of the ASAE, **44**(3), 721–729

Leemans V; Magein H; Destain M-F (2002). On-line fruit grading according to their external quality using machine vision. Biosystems Engineering, **83**(4), 397–404

Leemans V; Destain M-F (2004). A real-time grading method of apples based on features extracted from defects. Journal of Food Engineering, **61,** 83–89

Lu R (2003). Detection of bruises on apples using near-infrared hyper-spectral imaging. Transactions of the ASAE, **46**(2), 523–530

Ma L; Tao Y (2005). An infrared and laser range imaging system for non-invasive estimation of internal temperatures in chicken breasts during cooking. Transactions of the ASAE, **48**(2), 681–690

Mehl P M; Chen Y R; Kim M S; Chan D E (2004). Development of hyperspectral imaging technique for the detection of apple surface defects and contaminations. Journal of Food Engineering, **61,** 67–81

Park B; Lawrence K C; Windham W R; Buhr R J (2002). Hyperspectral imaging for detecting fecal and ingesta contaminants on poultry carcasses. Transactions of the ASAE, **45**(6), 2017–2026

Röhr A; Lüddecke K; Drusch S; Müller M J; Alvensleben R V (2005). Food quality and safety-consumer perception and public health concern. Food Control, **16**(8), 649–655

Wen Z; Tao Y (2000). Duel-camera NIR/MIR imaging for stem-end/calyx identification in apple defect sorting. Transactions of the ASAE, **43**(2), 449–452

Wolfe R R; Sandler W E (1985). An algorithm for stem detection using digital image analysis. Transactions of the ASAE, **28**(2), 641–644

Xing J; Bravo C; Jancsók P; Ramon H; De Baerdemaeker J (2005). Bruise detection on Golden Delicious apples by using hyperspectral imaging with multiple wavebands. Biosystems Engineering, **90**(1), 27–36

Yang Q (1993). Finding stalk and calyx of apples using structured lighting. Computers and Electronics in Agriculture, **8,** 31–42

Ying Y; Jing H; Tao Y; Zhang N (2003). Detecting stem and shape of pears using Fourier transformation and an artificial neural network. Transactions of the ASAE, **46**(1), 157–162